# Analysis of single nucleic acid molecules with protein nanopores — **Source link**

Giovanni Maglia, Andrew John Heron, David Stoddart, Deanpen Japrung ...+1 more authors

**Institutions:** University of Oxford

**Topics:** Nucleic acid quantitation and Nucleic acid

Related papers:

- Characterization of individual polynucleotide molecules using a membrane channel

- Single-nucleotide discrimination in immobilized DNA oligonucleotides with a biological nanopore

- Structure of Staphylococcal α-Hemolysin, a Heptameric Transmembrane Pore

- Single-molecule DNA detection with an engineered MspA protein nanopore

- Microsecond time-scale discrimination among polycytidylic acid, polyadenylic acid, and polyuridylic acid as homopolymers or as segments within single RNA molecules.

# ANALYSIS OF SINGLE NUCLEIC ACID MOLECULES WITH PROTEIN NANOPORES

Giovanni Maglia, Andrew J. Heron, David Stoddart, Deanpen Japrung, *and* Hagan Bayley

## Contents

Department of Chemistry, University of Oxford, Oxford, United Kingdom

## Abstract

We describe the methods used in our laboratory for the analysis of single nucleic acid molecules with protein nanopores. The technical section is preceded by a review of the variety of experiments that can be done with protein nanopores. The end goal of much of this work is single-molecule DNA sequencing, although sequencing is not discussed explicitly here. The technical section covers the equipment required for nucleic acid analysis, the preparation and storage of the necessary materials, and aspects of signal processing and data analysis.

## NOMENCLATURE

| | |
|---|---|
| ssDNA | single-stranded DNA |
| dsDNA | double-stranded DNA |
| $ddH_2O$ | distilled, deionized water |
| $f$ | normalized frequency of DNA interactions with pore (e.g., translocation events) in $s^{-1}\ \mu M^{-1}$ |
| $I_O$ | open pore current |
| $I_B$ | current through pore partially blocked by DNA |
| $I_F$ | fractional residual current, that is, $I_B/I_O$ |
| $I_{\%RES}$ | residual current as percentage of $I_O$, that is, $I_B/I_O \times 100$ |
| $\Delta I_{\%RES}$ | difference in $I_{\%RES}$ between residual currents (e.g., for two different DNAs) |
| $t_t$ | time taken for translocation of an individual nucleic acid molecule |
| $\bar{t}_t$ | mean time taken for translocation of a nucleic acid molecule |
| $t_D$ | dwell time of a nucleic acid molecule (not necessarily for a translocation event) |
| $\bar{t}_D$ | mean dwell time |
| $t_P$ | most probable dwell time or translocation time taken from the peak of a dwell time or translocation time histogram |
| $t_{ON}$ | interevent interval (e.g., time between translocation events) |
| $\bar{t}_{ON}$ | mean interevent interval |

# 1. BACKGROUND: ANALYSIS OF NUCLEIC ACIDS WITH NANOPORES

Nanopores have been used to detect and analyze single molecules (Bayley and Cremer, 2001; Branton *et al.*, 2008; Deamer and Branton, 2002; Dekker, 2007) and to investigate reaction mechanisms at the single-molecule level (Bayley *et al.*, 2008b). In this chapter, we focus on the analysis of nucleic acids with the protein pore formed by staphylococcal α–hemolysin (αHL). First, we present background on the wide variety of experiments that can be performed on nucleic acids. Second, we enlarge on technical aspects of these experiments that have proved useful in our laboratory.

In a nanopore experiment, a single pore is located in a thin barrier that separates two compartments (henceforth called *cis* and *trans*) containing aqueous electrolyte. An electrical potential is applied across the barrier and the flow of ions through the nanopore is monitored. Molecules of interest are investigated by analyzing the associated modulation of the ionic current when the molecules pass through the pore or interact with the lumen (Fig. 22.1A). In this way, information about the length of nucleic acid
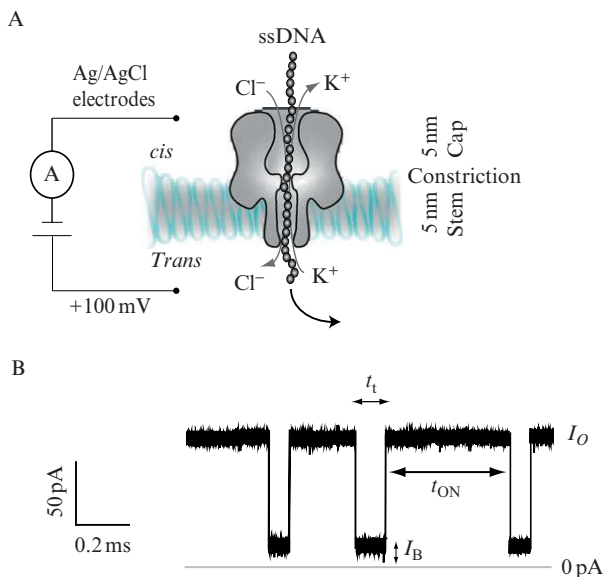


**Figure 22.1** Nanopore analysis of DNA. (A) Ag/AgCl electrodes are used to apply a potential (e.g., +100 mV) to drive DNA through an αHL nanopore embedded in a lipid bilayer and to measure the ionic current. (B) Typical trace for DNA translocating through a (wild-type) WT-αHL nanopore showing the translocation times ($t_t$), the residual current values ($I_B$), and the interevent intervals ($t_{ON}$) for individual DNA translocation events.

molecules and their base compositions is gathered. Duplex formation and dissociation, including unzipping in an applied potential, can be examined. The properties of enzymes and binding proteins associated with nucleic acids can also be determined. Stemming from this work, there is the potential to develop a cheap and fast technology to sequence single DNA molecules (Branton *et al.*, 2008), but we do not emphasize this aspect here.

The two most common classes of nanopores are protein pores in lipid bilayers (Fig. 22.1) or synthetic nanopores formed in a variety of thin films, including Si-based materials, PDMS (polydimethylsiloxane), and polycarbonate (Dekker, 2007; Rhee and Burns, 2007; Sexton *et al.*, 2007). Among the advantages of synthetic nanopores are that their dimensions can be adjusted during manufacture and that they can be produced as nanopore arrays. Protein nanopores also have significant advantages; in contrast with synthetic nanopores, their dimensions are reproducible and their structures can be precisely manipulated by site-directed mutagenesis and targeted chemical modification. The stability of solid-state pores in harsh environments is often mentioned as a key advantage, but it should be noted that the αHL pore can withstand denaturants (Japrung *et al.*, 2010), extremes of pH (Maglia *et al.*, 2009b), and temperatures up to ∼95 °C (Kang *et al.*, 2005), conditions adequate for the analysis of DNA.

Although we focus on the analysis of nucleic acids with the αHL nanopore, progress on DNA analysis with alternative protein pores is being made, notably with MspA from *Mycobacterium smegmatis* (Butler *et al.*, 2008). The experimental principles developed for αHL are valid in other cases.

## 1.1. Structure of the αHL nanopore

αHL is a heptameric protein that consists of a stem domain and a cap domain (Fig. 22.1) (Song *et al.*, 1996). The stem domain comprises 14 antiparallel $\beta$ strands (two per protomer) that form a roughly cylindrical water-filled channel of ∼2 nm internal diameter. The internal cavity, or vestibule, within the cap domain is roughly spherical with an internal diameter of ∼4.5 nm. The narrowest part of the interior of the pore is the constriction (1.4 nm in diameter), which is located between the cap and the stem domains. Under an applied potential, ions flow through the pore and the addition of single-stranded (ss)DNA to one side of the bilayer (typically the *cis* side) produces current blockades during the periods when a DNA molecule enters the pore (Fig. 22.1). Entry can result in a brief visit and then exit from the same side or translocation from the *cis* to the *trans* side of the bilayer. The dimensions of the pore are such that double-stranded (ds) DNA cannot pass through it (Kasianowicz *et al.*, 1996), although dsDNA can penetrate as far as the constriction when presented from the *cis* side (Maglia *et al.*, 2009b; Vercoutere *et al.*, 2001). While we most often refer to DNA in this review, the same principles apply to RNA analysis.

## 1.2. Nucleic acid analysis with αHL nanopores

In electrical recordings from planar bilayers, it is important that sign conventions are followed consistently. We use the following. The *cis* chamber is that to which the protein nanopore is added; after insertion, the cap domain is exposed to the *cis* electrolyte. The *cis* chamber is at ground and the transmembrane potential is given as the potential on the *trans* side (i.e., the *trans* potential minus the *cis* potential; the latter is "zero" in the present case). A positive current is one in which positive charge (e.g., $K^+$) moves through the pore from the *trans* to the *cis* side, or negative charge (e.g., $Cl^-$) from the *cis* to the *trans* side.

The information that can be extracted from a typical electrical recording of DNA translocation through an αHL nanopore is the mean translocation time ($\bar{t}_t$), the residual current level during translocation ($I_{\%RES}$), and the mean interevent interval ($\bar{t}_{ON}$), which is the inverse of the frequency of events ($f$), when $\bar{t}_{ON} \gg \bar{t}_t$ (Fig. 22.1B).

Translocation times of short single-stranded oligonucleotides ($<100$ nucleotides, nt) are described well by a Gaussian distribution with an exponential tail. The most probable translocation time ($t_P$) is given by the peak of the distribution (Meller *et al.*, 2000). At $+120$ mV and $25\,^{\circ}$C, the nucleic acid move through the pore at a speed of $1$–$22\ \mu$s per nt ($t_P$ divided by the number of nt). The speed depends on the base composition of the nucleic acid, with purine bases showing the shortest translocation times (Meller, 2003). In addition, $t_P$ decreases exponentially with the temperature or the applied potential (Meller *et al.*, 2000).

The frequency of occurrence of DNA translocation events increases with increased applied potential (Henrickson *et al.*, 2000), temperature (Meller *et al.*, 2000), or salt concentration (Bonthuis *et al.*, 2006). In addition, a threshold potential must be exceeded to observe DNA capture (Henrickson *et al.*, 2000) and even then capture is inefficient. Rough estimates suggest that, at voltages close to the threshold, about one DNA molecule in every 1000 that collide with the wild-type (WT)-αHL pore is captured (Meller, 2003). By contrast, at the highest accessible applied potentials (around $+300$ mV), $\sim 20\%$ of the collisions result in DNA translocation (Nakane *et al.*, 2002). However, the frequency of DNA capture can be improved by increasing the number of internal positive charges within the pore by site-directed mutagenesis, which also reduces the voltage threshold for DNA translocation through both the αHL (Maglia *et al.*, 2008) and MspA (Butler *et al.*, 2008) nanopores. The most likely mechanisms for the increased frequency of translocation are a strengthened interaction when DNA molecules sample the interior of the pore, increased electroosmotic flow, or a combination of the two that depends on the applied potential (Maglia *et al.*, 2008).

If nanopores are to be used to sequence DNA, single bases will most likely be identified at a recognition point within the nanopore by the extent

to which they reduce the ionic current, rather than their dwell times (Bayley, 2006). Therefore, if a large current flows during DNA translocation ($I_B$), the recognition of the bases is likely to be improved. The percent residual current ($I_{\%RES} = I_B/I_O \times 100$) shows less experiment-to-experiment variation than the residual current ($I_B$) and therefore it is the descriptor of choice. $\Delta I_{\%RES}$, the difference in $I_{\%RES}$ between residual currents (e.g., for two different DNAs), shows less variation still (Stoddart *et al.*, 2010). WT-αHL nanopores generally show relatively low $I_{\%RES}$ values (typically 10% in 1 $M$ KCl, at +120 mV), which depend on the nucleic acid used, with RNA generally blocking more current than DNA (Meller, 2003). $I_{\%RES}$ increases with increased applied potential (Stoddart *et al.*, 2009) and decreased salt concentration (D. Stoddart, unpublished data). Recent studies have shown that $I_{\%RES}$ also depends on the amino acid side chains that project into the lumen of the pore (Maglia *et al.*, 2008; Stoddart *et al.*, 2009). At +120 mV, additional positively charged residues in the barrel decrease $I_B$ by 60–80% relative to WT-αHL depending on the positioning of the charge (Maglia *et al.*, 2008), while the elimination of ionic interactions and the reduction of side-chain volume at the constriction, in the mutant E111N/K147N, increase $I_B$ by approximately twofold (Stoddart *et al.*, 2009).

## 1.3. Homopolymeric strand analysis with protein nanopores

Homopolymeric ssDNA or ssRNA blockades can be discriminated with (wild-type) WT-αHL nanopores by means of their residual currents ($I_B$) and translocation times ($t_P$). In 1 $M$ KCl and at +120 mV, poly-rA blockades show an $I_{\%RES}$ of 15% and a $t_P$ value of 22 $\mu$s per nt, which are readily distinguished from poly-rC blockades ($I_{\%RES}$ = 9% and 5%, and $t_P$ = 5.8 $\mu$s per nt) and from poly-rU blockades ($I_{\%RES}$ = 15% and $t_P$ = 1.4 $\mu$s per nt) (Akeson *et al.*, 1999). The DNAs, poly-dA and poly-dC, show different translocation times ($t_P$ = 1.9 and 0.8 $\mu$s per nt, respectively), but similar $I_{\%RES}$ values (12.6% and 13.4%, respectively) (Meller *et al.*, 2000), while poly-dU shows longer blockades than both poly-dC and poly-dA (Butler *et al.*, 2007). Although a fully convincing explanation has yet to be proposed, differences in translocation times and $I_B$ value of homopolymeric strands through αHL nanopores have been associated with differences in base pair-independent secondary structure including base stacking (Akeson *et al.*, 1999; Meller *et al.*, 2000).

The different extents of current blockade associated with homopolymeric RNA strands were exploited to detect the transition from poly-rA to poly-rC segments within the same molecule. When the translocation of poly-rA$_{30}$C$_{70}$ through the WT-αHL nanopore was investigated, ~50% of the events exhibited current steps that reflected the transition (Akeson *et al.*, 1999).

The mean translocation speed is constant for short DNAs (from 12 to 100 nt) (Meller and Branton, 2002; Meller *et al.*, 2001) and for poly-rU from 100 to 500 nt (Kasianowicz *et al.*, 1996). For oligonucleotides shorter than the length of the barrel ($N < 12$), the translocation speed decreases with increasing nucleotide length in a nonlinear fashion. Polynucleotides longer than 500 nt have not yet been carefully characterized.

## 1.4. Recognition of specific sequences and single base mismatches through duplex formation

αHL pores have been used to recognize specific DNA sequences and single nucleotide mismatches through duplex formation. Howorka *et al.* (2001) covalently attached an 8-nt oligonucleotide within the vestibule of an αHL pore. The complementary strand was then recognized by measuring the current blockade provoked by strand hybridization (Howorka *et al.*, 2001). Single nucleotide mismatches were identified because they produced shorter current blockades. Based on duplex lifetimes, the DNA–nanopores were able to discriminate mismatches between the oligonucleotide tethered to the pore and complementary 8-base sequences within DNA strands of up to 30 nt. In addition, the last three bases in a 9-nt DNA attached to the pore were sequenced by the sequential addition of known oligonucleotides (Howorka *et al.*, 2001). Vercoutere *et al.* (2001) detected single-base differences in short, blunt-ended DNA hairpin molecules with up to nine complementary bases. The entry of the hairpins into the vestibule of the αHL pore was accompanied by a characteristic current blockade. Once in the vestibule, the hairpins spontaneously dissociated and a current spike signaled the translocation of the DNA strand through the pore. Single-base mismatches were detected by reduced duplex lifetimes, which reflected the stabilities of the duplexes in solution (Vercoutere *et al.*, 2001). Nakane *et al.* (2004) used streptavidin to immobilize a biotinylated probe DNA molecule within the αHL pore (Fig. 22.2). The untethered end of the DNA strand entered the *trans* compartment at positive potentials, where it bound a complementary oligonucleotide to form a rotaxane. Reversal of the applied potential exerted a force on the duplex. A shorter mean time for dissociation by comparison with the value for a fully complementary pair was used to recognize single mismatches in probe-oligonucleotide duplexes (Nakane *et al.*, 2004).

## 1.5. Individual base recognition by αHL nanopores

The recognition of individual DNA bases during translocation is crucial if the sequencing of DNA molecules is to be achieved by using nanopores. However, at present, the translocation of nucleic acids through αHL nanopores is so rapid (1–22 $\mu$s per nt) that only artificially bulky bases
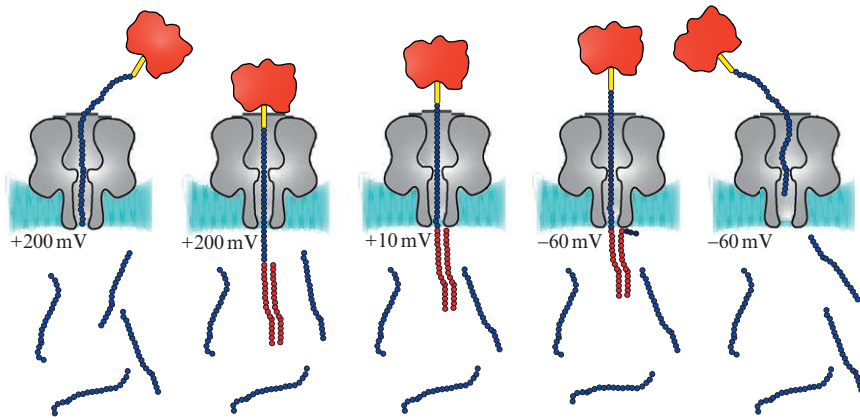
**Figure 22.2**  Detection of an ssDNA by hybridization. From left to right: A high applied potential (e.g., $+200$ mV) is used to capture a biotinylated DNA probe (complexed with streptavidin) within the αHL pore. The target DNA strand emerges on the opposite side of the bilayer where it forms a duplex, if it is recognized by a complementary strand. The voltage is lowered to $+10$ mV. If a duplex has been formed, the probe DNA remains in the pore as a rotaxane. If a duplex has not formed, the probe DNA escapes under the low applied potential. To measure the strength of the duplex, eject the probe DNA and begin a new cycle, the applied potential is stepped to $-60$ mV.

(Mitchell and Howorka, 2008) or the transition between homopolymer stretches of $\sim 30$ nt can be detected (Akeson *et al.*, 1999). Therefore, to test the feasibility of base detection, DNA strands have been immobilized within the αHL pore by using terminal hairpins (Ashkenasy *et al.*, 2005) (Fig. 22.3C). Because the hairpin might interfere with recognition (Fig. 22.3A), recent work has exploited the interaction between a biotinylated oligonucleotide and streptavidin to immobilize DNA strands (Purnell and Schmidt, 2009; Stoddart *et al.*, 2009) (Fig. 22.3B). In our work, the ability of the αHL pore to discriminate individual bases was investigated by sampling several DNA molecules in which the position of a single base was altered in an otherwise identical homopolymeric background (Fig. 22.3C). While Ghadiri and coworkers were able to identify a recognition point at the *trans* entrance of the αHL nanopore that could discriminate a single dA in a poly-dC background (Ashkenasy *et al.*, 2005), the biotinylated oligonucleotides were used to sample the entire length of the pore (Stoddart *et al.*, 2009). αHL was found to contain three broad recognition sites. When an engineered pore (E111N/K147N) was used, with enhanced current flow when DNA occupies the pore ($I_B$), all four DNA bases could be distinguished in a poly-dC background. Individual base differences could also be detected in a heteropolymeric DNA strand (Stoddart *et al.*, 2009).
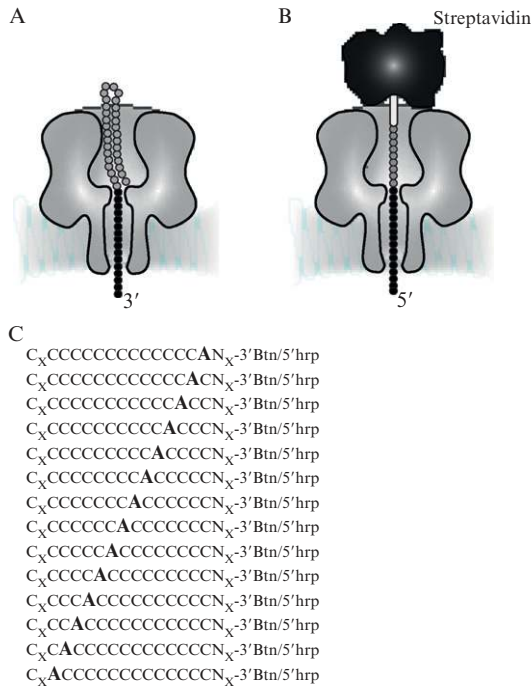
A

B                    Streptavidin

3′                      5′

C

$C_X$CCCCCCCCCCCCCC**A**$N_X$-3′Btn/5′hrp
$C_X$CCCCCCCCCCCCC**A**C$N_X$-3′Btn/5′hrp
$C_X$CCCCCCCCCCCC**A**CC$N_X$-3′Btn/5′hrp
$C_X$CCCCCCCCCCC**A**CCC$N_X$-3′Btn/5′hrp
$C_X$CCCCCCCCCC**A**CCCC$N_X$-3′Btn/5′hrp
$C_X$CCCCCCCCC**A**CCCCC$N_X$-3′Btn/5′hrp
$C_X$CCCCCCCC**A**CCCCCC$N_X$-3′Btn/5′hrp
$C_X$CCCCCCC**A**CCCCCCC$N_X$-3′Btn/5′hrp
$C_X$CCCCCC**A**CCCCCCCC$N_X$-3′Btn/5′hrp
$C_X$CCCCC**A**CCCCCCCCC$N_X$-3′Btn/5′hrp
$C_X$CCCC**A**CCCCCCCCCC$N_X$-3′Btn/5′hrp
$C_X$CCC**A**CCCCCCCCCCC$N_X$-3′Btn/5′hrp
$C_X$CC**A**CCCCCCCCCCCC$N_X$-3′Btn/5′hrp
$C_X$C**A**CCCCCCCCCCCCC$N_X$-3′Btn/5′hrp
$C_X$**A**CCCCCCCCCCCCCC$N_X$-3′Btn/5′hrp

**Figure 22.3** Single base recognition in immobilized DNA strands. (A) The transloca-tion of a DNA strand can be arrested by using a terminal DNA hairpin. (B) Alterna-tively, the translocation of a biotinylated DNA strand can be halted by preincubating the ssDNA with streptavidin. The grey circles indicate the DNA that is in the vestibule and the black circles are the DNA bases that span the barrel of the pore. (C) The barrel of the pore can be sampled by measuring the current blockades provoked by DNA sequences in which the location of a single base is moved within an otherwise identical background. Hrp, hairpin; Btn, biotinylated linker; $N_X$, nucleotides that are in the vestibule of the pore; $C_X$, nucleotides that protrude through the *trans* entrance of the pore.

## 1.6. Control of DNA translocation through nanopores

Controlling the speed at which DNA translocates through a pore is perhaps the single most important challenge that has to be overcome in nanopore sequencing (Branton *et al.*, 2008). At high sampling rates, noise levels are too high for base discrimination. A recent paper estimates that 98% of the small current differences observed for the four DNA nucleotides could be discriminated by an αHL nanopore assuming a mean dwell time of 10 ms (Clarke *et al.*, 2009), but this is at least 3 orders of magnitude longer than the transit time for individual bases in freely translocating ssDNA. Several attempts have been made to reduce the DNA translocation speed. For example, it has been shown recently that increasing the viscosity of the

sample solution by adding 63% (v/v) glycerol to the aqueous electrolyte can slow down DNA translocation through αHL nanopores by more than an order of magnitude, but at the expense of a 10-fold decrease in the unitary conductance of the pore (Kawano *et al.*, 2009). In efforts to increase the local viscosity, but preserve the conductance of the pore, a positively charged dendrimer with a hydrodynamic volume of 4.2 nm (Martin *et al.*, 2007) and uncharged PEG molecules of similar size (G. Maglia, unpublished data) were covalently attached inside the vestibule of the αHL pore. The modified nanopores showed a conductance that was roughly half that of the WT-αHL pore. However, both polymers almost completely inhibited the passage of nucleic acids through the pore, rather than slow their movement. Attempts to engineer the internal positive charge of the αHL pore to form "molecular brakes" to reduce the speed of ssDNA translocation have also been made (Rincon-Restrepo, in preparation). Modified versions of the pore were prepared with up to seven internal rings of seven arginine residues. Although the translocation speed was reduced by more than 2 orders of magnitude, the resulting $I_B$ values were too low to allow for discrimination of individual bases. Optical and magnetic traps have also been used to move DNA strands through solid-state nanopores (Keyser *et al.*, 2006; Peng and Ling, 2009), but so far these have been long double-stranded DNAs. Due to the instability of the lipid bilayer and the diffusion of nanopores within it, these techniques cannot be easily implemented with biological nanopores.

Ultimately, DNA-processing enzymes will most likely be used to control DNA translocation through biological pores. ExoI–ssDNA complexes gave current blockades that were approximately fivefold longer and showed a higher $I_B$ value than the current blockades produced by free ssDNA under the same conditions (+180 mV, 1 $M$ KCl) (Hornblower *et al.*, 2007). The disappearance of the long current blockades after the addition of $Mg^{2+}$, which triggers the activity of the enzyme, confirmed that these blockades were due to DNA in ExoI–ssDNA complexes entering the nanopore. But, the enzymatically driven movement of DNA was not demonstrated in this work. In a similar approach, the interaction of RNA with the αHL pore was monitored in the presence of P4 ATPase, a motor protein from bacterio-phage $\phi$8, but again the movement of the nucleic acid could not be shown (Astier *et al.*, 2007). Recently, the activity of a DNA polymerase was monitored with single base resolution by using an αHL nanopore (Cockroft *et al.*, 2008). A DNA strand was immobilized within the pore by threading a streptavidin·biotin–phosphoPEG–ssDNA complex through the *trans* entrance under a negative potential (Fig. 22.4). DNA primers (to form a rotaxane) and *TopoTaq* DNA polymerase were then added to the *cis* side and single-nucleotide primer extensions were identified by the current changes caused by the movement of phosphoPEG into the barrel of the pore after the addition of dNTPs (Fig. 22.4). Up to nine successive steps were
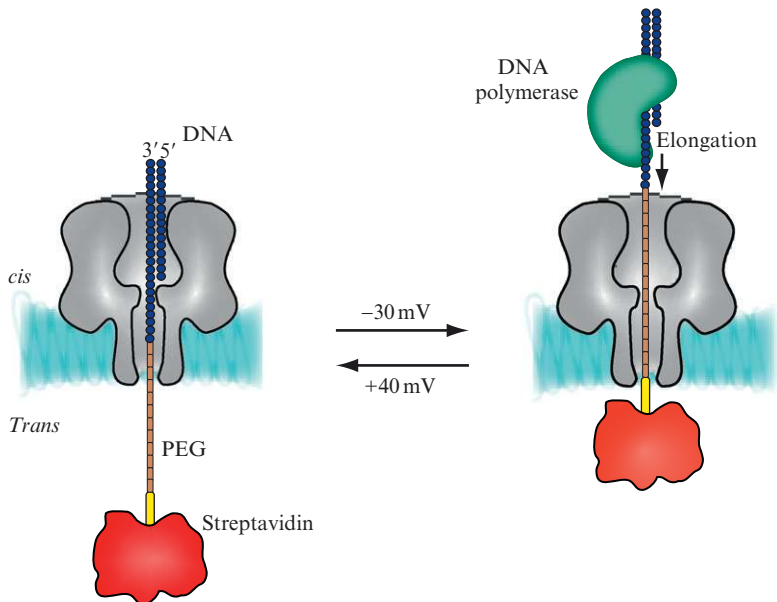
**Figure 22.4** Single nucleotide extension monitored with a protein nanopore. (Left) The monitoring configuration. A phosphoPEG sequence occupies a fraction of the barrel of the αHL pore and modulates the ionic current to a level that depends on the extent to which the primer has been elongated. (Right) Elongation configuration. dsDNA is accessible to the DNA polymerase. Elongation by a single nucleotide is controlled by the identity of the dNTPs in solution. The activity of the DNA polymerase can be monitored by stepping the potential between $+40$ and $-30$ mV.

observed by switching the potential between $-30$ mV (a potential at which elongation was possible) and $+40$ mV (the potential used to monitor the elongation steps). Future efforts will be directed toward combining such an elongation device with an engineered αHL pore capable of base identification.

## 2. ELECTRICAL RECORDING WITH PLANAR LIPID BILAYERS

Protein nanopores employed for DNA analysis must be reconstituted into artificial bilayers that mimic biological membranes. We carry out our experiments with planar lipid bilayers, examining single pore under *in vitro* conditions where all the constituents of the system are carefully controlled. "Single-channel" experiments require sensitive equipment to measure the small currents passed by individual protein pores. There is a wealth of good literature detailing the various aspects of setting up such equipment and

carrying out experiments on single protein channels and pores (see, e.g., The Axon Guide: www.moleculardevices.com/pages/instruments/axon_guide. html) (Hanke and Schlue, 1993; Miller, 1986; Sakmann and Neher, 1995), so here we just cover the specific apparatus and procedures employed in our laboratory for examining the interaction of DNA with the αHL pore.

## 2.1. Electrical recording equipment

Single-channel electrical measurements can be carried out with a range of equipment, both commercial and custom built. We use Axopatch 200B patch–clamp amplifiers (Molecular Devices) with 16-bit digitizers (132x or 1440A, Molecular Devices). DNA measurements are typically acquired in voltage-clamp mode using resistive WHOLE-CELL ($\beta = 1$) headstage settings. In voltage–clamp mode, the applied voltage is fixed, and the transmembrane current required to maintain that voltage is measured. Voltage clamping does not mimic a process found in nature, but many of the interactions of DNA with the αHL pore are voltage dependent, so it is imperative to control the applied potential. Furthermore, in this mode no capacitive transients are produced (except when changing the applied voltage), and the current flow is proportional to the conductance of the channels.

The Axopatch 200B has a recording bandwidth of 100 kHz, and the digitizers have a maximum sampling rate of 250 kHz per channel, which determines the maximum temporal resolution(4 $\mu$s). Amplitude resolution is primarily limited by the noise in the system. Planar bilayers are prone to relatively high background current noise (e.g., $>1$ pA RMS at 10 kHz) that can obscure small current steps (The Axon Guide) (Mayer *et al.*, 2003; Wonderlin *et al.*, 1990). Signal-to-noise can be improved by applying low-pass filtering, at the expense of a loss of temporal resolution. Therefore, although the electronics can acquire in the microsecond regime (freely translocating nucleic acids pass at $\sim$1–22 $\mu$s per nt), in practice there is a balance between acquiring fast enough to observe the events of interest, and low-pass filtering to observe small amplitude current differences.

There are three main sources of internal noise in a planar bilayer system, in increasing order of magnitude (The Axon Guide) (Mayer *et al.*, 2003; Wonderlin *et al.*, 1990): (1) noise originating in the acquisition electronics, (2) noise from clamping the thermal voltage noise in the access resistance (i.e., the resistance of the solutions and electrodes in series with the bilayer) across a large capacitance bilayer, and (3) noise from the nanopore itself. There are various strategies for reducing noise that are well covered in the literature (The Axon Guide) (Mayer *et al.*, 2003; Wonderlin *et al.*, 1990). Access resistance can account for substantial noise in planar bilayer systems in the absence of a pore (Wonderlin *et al.*, 1990). The access resistance can be reduced by: (1) using higher salt solutions in the *cis* and *trans* compartments, (2) using larger area electrodes, and (3) reducing the resistance of the agar

bridges (discussed below). The use of suitable aperture materials is also important for reducing dielectric noise (e.g., PTFE films produce lower noise than some other plastics; Mayer *et al.*, 2003; Wonderlin *et al.*, 1990). However, the single most effective means of reducing noise in the absence of a pore is to reduce the size of the bilayer and hence its capacitance (The Axon Guide) (Mayer *et al.*, 2003; Wonderlin *et al.*, 1990). Nevertheless, in practice, the largest source of noise is from the protein pore itself. Protein-derived noise arises from extremely fast fluctuations in conformation and charge states inside a pore (Bezrukov and Kasianowicz, 1993; Korchev *et al.*, 1997). The noise is dependent on physical conditions (pH, temperature, salt concentration, etc.), and for αHL we typically observe RMS noise that is two to three times greater than the noise from the bilayer alone.

## 2.2. Faraday enclosure

Electrical recording experiments should be carried out in a conducting enclosure (a Faraday cage) to shield the sensitive acquisition electronics from external radiative electrical noise. We typically use steel or aluminum boxes $\sim 50 \times 50 \times 50$ cm in dimensions with rigid side walls $>1$ mm thick. The boxes are grounded via the common ground in the patch-clamp amplifier (www.moleculardevices.com). Vibration isolation is an important consideration (The Axon Guide). External noise (e.g., from heavy machinery) can be transmitted through a laboratory bench into the box and result in substantial noise in the signal. Therefore, we mount our Faraday cages on pneumatic antivibration tables or soft supports (e.g., partially inflated soft rubber tubing). Unfortunately, antivibration tables do little to prevent sensitivity to environmental noise (i.e., loud noises, or even talking), as the large surfaces of the boxes pick up vibrations in the air. Although the Faraday cage might be housed inside an acoustically isolated enclosure, this source of noise can simply be eliminated by using a Faraday cage with stiff or absorbent walls that are well damped against vibrations. Finally, it is essential that the electrodes within the box are: (1) as short as possible (to reduce access resistance, input capacitance, and the reception of radiated noise) and (2) firmly secured to prevent their vibration.

While a Faraday cage is effective at isolating the system from external noise, care must be taken not to introduce internal sources of noise. As a result, any internal equipment (e.g., stirrers, peltier heaters, etc.) needs to be carefully shielded and should ideally run off a DC battery inside the Faraday cage.

## 2.3. Preparation of electrodes

Ag/AgCl electrodes are most commonly employed in bilayer recording due to their long-term chemical stability, reversible electrochemical behavior, predictable junction potentials, and superior low-noise electrical performance.

However, it should be noted that Ag/AgCl electrodes only perform well in solutions containing chloride ions. For experiments involving asymmetric solutions (where the chambers contain chloride ions at different concentrations), agar bridges (as discussed later) are used to prevent substantial liquid junction potential offsets (The Axon Guide).

Ag/AgCl electrodes are typically prepared from Ag wire by either: (1) electroplating in HCl solution, (2) dipping in molten AgCl, or (3) treatment with a weak hypochlorite solution (The Axon Guide) (Purves, 1981). Our preferred approach is an overnight treatment with hypochlorite, as this produces long lasting electrodes with a thick coating of AgCl. We make our electrodes from 1.5 mm diameter silver wire ($>99.99\%$, Sigma–Aldrich), using lengths of $\sim$10 mm (Fig. 22.5). These electrodes have a large reactive surface area, which prolongs their working life and minimizes the access resistance. Before treatment, the electrodes are thoroughly cleaned and roughened by abrasion (e.g., with a wire brush or glass paper), and then immersed in 1–5% (w/v) NaClO (Fisher Scientific) in water. After treatment, the electrodes are rinsed with distilled water. The electrodes are prepared and stored in the dark to prevent UV conversion of AgCl back to Ag. In our experience, good electrodes have a rough texture and a dull gray color (Fig. 22.5).

The use of a 3 $M$ KCl/agar bridge between an electrode and the chamber solution is recommended for all experiments, but in particular for experiments carried out under asymmetric salt conditions to reduce junction potential offsets. The 3 $M$ KCl filling solution also reduces the access resistance. Another advantage of the agar bridge is that it prevents Ag$^+$ ions from the electrode leaching into the solution, which can adversely affect the activity of some protein pores. To create the agar bridges, we incorporate our 1.5 mm Ag/AgCl electrodes into 200 $\mu$l pipette tips (Gilson, USA) filled with (initially) molten agar (3% (w/v) low melt agarose



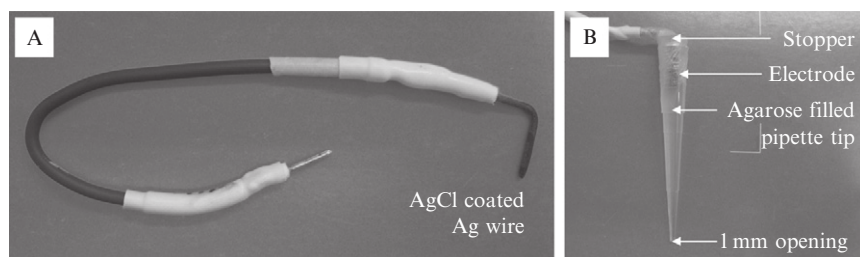**Figure 22.5** Ag/AgCl electrodes. **(A)** Photograph of an Ag/AgCl electrode, prepared by hypochlorite treatment of a short piece ($\sim$10 mm) of 1.5 mm–diameter Ag wire (soldered onto standard electrical wire). **(B)** To make agar bridges, we incorporate our electrodes into 200 $\mu$l pipette tips filled with agar (3%, w/v, 3 $M$ KCl in unbuffered ddH$_2$O), sealing the top with a rubber stopper and parafilm.

in 3 $M$ KCl in pure water), with a rubber stopper as a seal (Fig. 22.5). In addition, the opening of the pipet connecting to the bulk chamber solution should not be too small (we recommend an opening of $>1$ mm diameter).

Immediately before use, the electrodes are electrically balanced in symmetric solutions of the experimental buffer (e.g., 1 $M$ KCl, 25 m$M$ Tris–HCl, pH 8.0) by using the pipet offset function on the patch-clamp amplifier. Little to no potential adjustment is required for good electrodes. A sign of poor or degraded electrodes is the development of white patches and a requirement to rebalance the potential offset.

## 2.4. Chambers

We use open planar bilayer chambers for the majority of our DNA experiments. However, in some cases, in particular where limited quantities of reagents are available, we also make use of droplet interface bilayers that have solution volumes of $<200$ nl (Bayley *et al.*, 2008a). Open chambers come in a wide variety of shapes and formats, with vertical or horizontal bilayers and solution volumes ranging from 50 $\mu$l to 1 ml. Although commercial options are available (e.g., Warner Instruments), we use custom vertical bilayer devices machined from Delrin (Fig. 22.6), where the two compartments of 0.5–1.0 ml are separated by a 20 $\mu$m-thick PTFE film (Goodfellow, UK). In this format, both the *cis* and *trans* solutions are easily accessed for the purposes of adding reagents or perfusion.
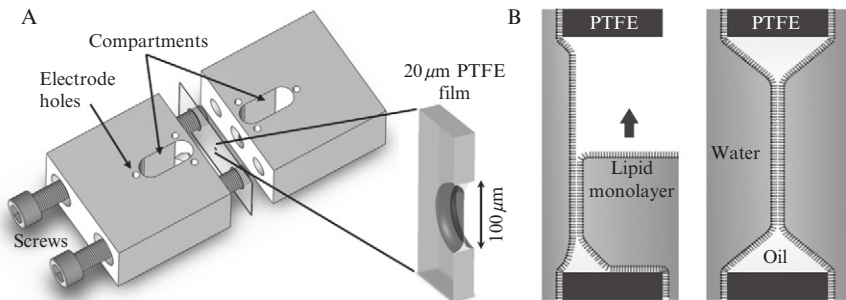


**Figure 22.6** Planar bilayer formation. (A) We use custom vertical planar bilayer chambers, with two 1 ml compartments separated by a 20-$\mu$m PTFE film, shown here in an exploded view. The two halves are fastened together with screws, clamping the PTFE film between them. The apparatus is sealed with silicone glue (Sylgard 184, Dow Corning) to ensure water-tightness. The PTFE film contains a central aperture $\sim$100 $\mu$m diameter, across which the bilayer is formed. (B) The bilayer is formed by the Montal–Mueller method. The aperture is pretreated with an oil (e.g., hexadecane), and the bilayer is then formed by flowing Langmuir–Blodgett lipid monolayers over both sides of the aperture.

The only path between the two compartments is a central aperture in the PTFE film across which the bilayer is formed (Fig. 22.6A, enlargement). The diameter depends on the size of bilayer required, and is typically $\sim 100$ $\mu$m. While there are many approaches for producing small apertures (Wonderlin *et al.*, 1990), we favor ''zapping'' the films with a custom high-voltage spark generator (producing a spark $\sim 15$ mm long at a frequency of $\sim 1$ Hz). Commercial products are available (e.g., Daedelon, USA). To control the location of the aperture, the Teflon film is weakened at the desired point by gently indenting with a sharp needle. The spark passes through this weakness, and the high temperature causes localized melting, which produces a perfectly round aperture. The aperture is sparked several times until the desired diameter is achieved (as measured under a microscope with a graticule). This technique produces high quality apertures with reproducible dimensions (typically $>50$ and $\pm 10$ $\mu$m) (Mayer *et al.*, 2003).

Reducing bilayer size, and hence capacitance, reduces noise. However, this must be balanced against the practical necessity of creating bilayers reproducibly (bilayers that are too small are often occluded by enlargement of the annulus) and the difficulty of inserting channels into overly small bilayers. A good compromise is to use bilayers with a capacitance of $\sim 60$–100 pF, which corresponds to a diameter of $\sim 105$–135 $\mu$m (DPhPC/hexadecane, assuming a specific capacitance of 0.70 $\mu$F cm$^{-2}$; Peterman *et al.*, 2002).

## 2.5. Preparing bilayers

Planar bilayers are typically created across small apertures in a plastic film by variants of two main approaches (White, 1986). In the first, the bilayer is created by directly painting a lipid/oil solution (e.g., 5% (w/v) of DPhPC in hexadecane) around the aperture before adding the aqueous solution. This thick lipid/oil film spontaneously thins and after a few minutes forms a bilayer due to Plateau–Gibbs suction (Niles *et al.*, 1988). In the second approach, the aperture is first pretreated with the oil (e.g., hexadecane), and then the bilayer is formed by flowing Langmuir–Blodgett lipid monolayers across both sides of the aperture (Fig. 22.6B) (Montal and Mueller, 1972; White *et al.*, 1976). In both approaches, the oil (generally an *n*-alkane such as decane or hexadecane) is extremely important, as it creates an annulus around the rim of the aperture, which allows the bilayer to form an interface with the plastic film (Plateau–Gibbs border). We favor the second ''Montal–Mueller'' approach. The primary advantages of this technique are that the bilayers are quick to form (with the painting approach it can take tens of minutes for the bilayer to spontaneously thin), and asymmetric bilayers can be created if the two compartments contain lipids of a different composition.

Briefly, we pretreat the aperture with hexadecane by the direct application of a single drop ($\sim 5\ \mu$l) of 10% (v/v) hexadecane in pentane. After the pentane has evaporated, both compartments of the chamber are filled with the buffered aqueous electrolyte and the electrodes are connected. The aperture should be free of excess oil, so that an electrical current can be measured between the compartments. (At zero applied potential on the amplifier, there remains a very small potential difference between the compartments.) In the case of blockage, excess oil can be removed by gently pipetting solution at the aperture. A small drop ($\sim 5\ \mu$l) of lipid in pentane solution (e.g., DPhPC, 10 mg ml$^{-1}$) is then applied directly to the top of the aqueous phase. After waiting $\sim 1$ min for the pentane to evaporate fully, solution is pipetted from the bottom of a compartment to lower the lipid monolayer at the water–air interface past the aperture level. The solution level is then slowly raised back above the aperture. After repeating this procedure several times in each compartment, a bilayer forms, and the electrical current drops to zero. We measure the capacitance, as described later, to judge the size and quality of the bilayer.

We use DPhPC bilayers with hexadecane as the oil in most of our studies. DPhPC has ideal bilayer forming properties. It exists in the fluid lamellar phase across a wide temperature range ($-120$ to $+120\ °$C) (Hung *et al.*, 2000; Lindsey *et al.*, 1979), and it is stable to oxidation. Planar bilayers can, however, be prepared from a wide range of phospholipids or phospholipid mixtures. These can have zwitterionic or charged headgroups, and may contain additives such as cholesterol. The correct lipid mixture may be essential for certain proteins to function (e.g., mechano-sensitive channels; Phillips *et al.*, 2009). The phospholipid mixture usually, but not always (Krasne *et al.*, 1971), has fluid lamellar properties under the conditions of the experiment. Many oils can be used to interface the bilayer with the aperture (*n*-alkanes, squalene, etc.), but experimentalists should be aware that the shorter chain *n*-alkanes (e.g., decane) interdigitate into the bilayer leading to increased bilayer thickness (White, 1975, 1986). Although this is not important for a robust pore such as αHL, bilayer thickness differences can affect the properties of membrane proteins (Phillips *et al.*, 2009). Hexadecane produces bilayers with little oil content (White, 1975, 1986).

A standard cleaning routine is used between experiments: first rinsing with large amounts of water, then repeated steps of distilled water rinses followed by 100% ethanol rinses. Finally, the chambers are thoroughly dried under a stream of nitrogen. When required, we also employ detergent washing steps, NaOH (1 *M*) or HCl (1 *M*) washes, or rinsing with an EDTA solution (e.g., 10 m*M*) to remove traces of divalent metal ions.

### 2.5.1. Bilayer stability

The planar bilayers we have described typically have lifetimes of a few hours and can withstand constant applied potentials of 200–300 mV. Smaller bilayers ($<100\ \mu$m diameter) are much less susceptible to pressure variations

and mechanical shock, and are therefore longer lived. DPhPC bilayers are stable up to $\sim$100 °C (Kang *et al.*, 2005). In certain cases, alternative oils should be used. For example, hexadecane is frozen below 18 °C, and hexadecene or shorter chains alkanes can be employed at low temperatures. Planar bilayers are also able to withstand substantial osmotic gradients arising from the use of asymmetric salt conditions (we often use asymmetric solutions of 150 m$M$/1 $M$ salt to measure ionic charge selectivity), although the solutions can be balanced if instability occurs by the addition of an osmolyte (e.g., sucrose) to the low-salt compartment.

### 2.5.2. Measuring bilayer capacitance

It is important to measure bilayer capacitance, because pores will not insert into misformed bilayers. There are a number of ways of determining capacitance (for reviews see Gillis, 1995; Kado, 1993). One of the most versatile and straightforward is the application of voltage ramps to elicit constant capacitive currents (Fig. 22.7). Since current ($I$) is proportional to the rate of change of voltage (d$V$/d$t$) for a capacitor ($I = C \times$ d$V$/d$t$), an applied triangular voltage waveform produces a square-wave current output (i.e., d$V$/d$t$ = constant, for each sweep), which can be used to determine bilayer capacitance (Fig. 22.7). We use commercial analog waveform generators, inputting a triangular wave ($\sim$20 Hz) into the patch–clamp amplifier (front-switched input on an Axopatch 200B amplifier). We directly calibrate the input waveform by using a 100 pF bilayer model cell (MCB-1U, Molecular Devices), so that 100 pA = 100 pF. This approach provides a visual measurement of capacitance, which is useful
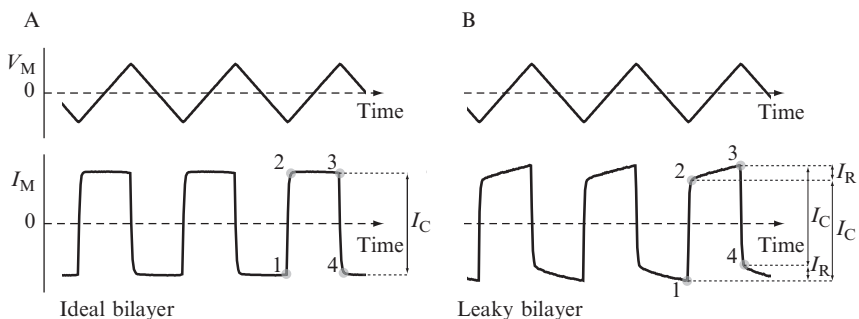


**Figure 22.7**  Measuring bilayer capacitance. A triangular-wave voltage input applied across a capacitor produces a square-wave current output. (A) Bilayer capacitance can be determined by measuring the peak-to-peak magnitude of the square-wave current output ($I_C$). (B) A leak in the bilayer is visualized by the triangular ohmic deviation ($I_R$) from the ideal square-wave.

for determining the quality of a bilayer seal (leaks are readily apparent as a triangular deviation from the ideal square-wave output ($I_R$ in Fig. 22.7)).

## 2.6. Inserting pores and adding DNA

In the case of αHL, there are several ways to insert the pore into a planar bilayer. αHL is a toxin that assembles spontaneously from water-soluble monomers, so pores can be formed by adding monomeric αHL directly to the chamber. However, it is often difficult to obtain a single channel by using this approach (many pores tend to insert if the monomer remaining after a single pore has formed is not removed by perfusion), and we also find that the αHL pores formed from monomers have substantial pore-to-pore variability (discussed below). We therefore prefer to use preoligomerized protein in a detergent-solubilized form (e.g., after extraction from an SDS–polyacrylamide gel as described below). Typically $\sim 0.2$ $\mu l$ of SDS–solubilized heptamer ($\sim 1$ ng $\mu l^{-1}$) is manually ejected from a pipette very close to the bilayer beneath the surface of the solution in the *cis* compartment. The solution in the compartment is then stirred gently with a small magnetic stirrer bar until a single insertion event is observed. Electrical recordings are noisy while stirring, as the changing magnetic field produced by the rotating stirrer and stirrer bar induces currents in the electrodes, and stirring is discontinued for the rest of the experiment, unless additions are made to a compartment. Although the protein concentration can be reduced to improve the chances of obtaining a single insertion event, this often requires waiting a considerable length of time. Alternatively, a higher concentration of protein can be added to reduce the time to insertion, followed by prompt perfusion (see below) to remove free protein.

Two other methods of inserting protein employed in our laboratory are vesicle fusion (better suited to proteins that are unstable in detergent) (Morera *et al.*, 2007) and direct introduction with probes (Holden and Bayley, 2005; Holden *et al.*, 2006), which is also suited to unstable proteins or proteins of which only small quantities are available.

DNA, RNA, or other analytes are added directly to the chamber solutions from stocks (typically 100 $\mu M$ in double-distilled water (ddH$_2$O) or 10 m$M$ Tris-HCl, 100 $\mu M$ EDTA, pH 8.0) by pipet. Mixing is achieved by stirring the chamber solution for up to 1 min (using a 5 mm stirrer bar in the bottom of the compartment). Depending on the experiment, we typically add oligonucleotides to the 1 ml compartment solution from 100 $\mu M$ stocks to give final concentrations of 10 n$M$ to 2 $\mu M$. The electrode compartments may represent an appreciable dead volume (e.g., 5% of the total volume), which must be taken into account for quantitative work. Better still, the concentration of a DNA or RNA in a compartment should be checked after an experiment, for example, by UV spectrometry.

## 2.7. Perfusion

We use perfusion to remove free protein from the bulk solution once a single pore has inserted, and to change the solution conditions or analytes in the system while retaining the same pore in the bilayer. We perfuse our devices by manual pipetting (removing some solution and replacing it with fresh solution) or with push–pull syringe drivers (e.g., PHD 2000, Harvard Apparatus) that exchange the solution at rates of $\sim 1$ ml min$^{-1}$. It should be noted that solution-filled perfusion tubing entering the Faraday cage acts as an antenna and picks up radiative noise that can prevent useful recording while the perfusion equipment is connected. If this is a problem, drip-feed perfusion can be employed, where the air pocket breaks the electrical continuity in the tubing.

## 3. NANOPORES

### 3.1. Nanopore preparation

While monomeric αHL can be obtained commercially, we recommend the use of heptamers carefully prepared in the laboratory. This is of course essential for heteroheptamers with defined subunit combinations (Miles *et al.*, 2002), but we have also found that preassembled homoheptamers give more consistent results than monomers in bilayer experiments.

In our laboratory, αHL homoheptamers used in single-channel recording experiments are usually prepared from αHL monomers expressed by *in vitro* transcription and translation (IVTT). Heptamers are formed by incubating the monomers with rabbit red blood cell membranes and purified by SDS–PAGE (Cheley *et al.*, 1999). The concentration of heptamer after purification is typically $\sim 1$ ng $\mu l^{-1}$. Alternatively, if a higher concentration of protein is required (e.g., for a protein that inserts poorly; Maglia *et al.*, 2009a), αHL monomers can be expressed in *Escherichia coli* or *Staphylococcus aureus* bacterial expression systems (Cheley *et al.*, 1997). In these cases, monomers are purified by ion exchange chromatography before incubation with a surfactant (6.25 m$M$ DOC; Bhakdi *et al.*, 1981; Tobkes *et al.*, 1985) to trigger the heptamerization process. Heptamers are then separated from monomers by size-exclusion chromatography (Cheley *et al.*, 1997). These procedures are more laborious, but αHL heptamers at concentrations of 1–5 mg ml$^{-1}$ can be obtained.

### 3.2. Nanopore storage

αHL heptamers are usually stored at $-80\ ^\circ$C in 10 m$M$ Tris–HCl buffer at pH 8.0, containing 100 $\mu M$ EDTA. Heptamers prepared from monomers produced from bacterial expression systems will also contain surfactants

(usually 1.25 m$M$ DOC), while heptamers prepared from αHL monomers obtained by IVTT are likely to contain small amounts of polyacrylamide and SDS that are carried over from the SDS-PAGE purification. Polyacrylamide can be removed by using a small size-exclusion column (e.g., P6 Micro Bio-Spin chromatography columns, Bio-Rad), but it usually does not interfere with single-channel recording experiments.

To obtain single channels, protein solutions obtained after IVTT expression, assembly, and electrophoretic purification are usually diluted 10-fold in buffer or ddH$_2$O, and 0.2 $\mu$l is added to the buffer in the planar bilayer chamber. At this point, residual SDS is well below its critical micelle concentration (CMC). During an experiment, solutions containing αHL proteins are kept on ice. αHL preparations can be stored at 4 °C for short-term use (less than a week), but the protein slowly loses activity. Multiple freeze/thaw cycles also reduce protein activity. When a reactive group is present (e.g., an oxidation sensitive cysteine residue), the protein must be handled with particular care and long-term storage at $-80$ °C is usually limited to a few months.

## 3.3. Measurements with nanopores

Purified WT heptamers form pores that have a high unitary conductance ($\sim 1$ nS at $+100$ mV in 1 $M$ KCl solution). WT-αHL pores show no gating events (openings and closings of the pore), unless the applied potential is high (more than $\pm 180$ mV), and even then the events are rare (generally less than 1 min$^{-1}$). Pore-to-pore variation of the unitary conductance is generally within 5% of the mean. However, very occasionally ($< 5\%$ of the cases), the pores show a high level of gating or have a dramatically reduced conductance. These cases probably arise from misfolded or misassembled heptamers and are discarded. αHL monomers, rather than purified heptamers, can also be used in single-channel recordings. However, a much greater number of the pores formed from monomers (from 20% to 50%, depending on the batch) show a reduced conductance or gating events. The use of heptamers purified by SDS-PAGE is therefore recommended. Over the course of long experiments ($> 30$ min), the open pore current can drift due to evaporation of the solutions or exhaustion of the Ag/AgCl electrodes. It is recommended, therefore, always to use agarose bridges around the electrodes and to minimize the surface area of the solutions. If lids are used, care must be taken to prevent a short circuit through a film of electrolyte. Layers of oil can be placed on the surfaces of the chamber solutions, but then a complete clean-up will be required if the bilayer is reformed.

The αHL pore can be altered by site-directed mutagenesis to give improvements in $f$ and $I_B$. Alteration of the lumen of the αHL pore by site-directed mutagenesis generally produces nanopores that have similar unitary conductance ($I_O$) values to that of WT-αHL (Gu *et al.*, 2001;

Stoddart *et al.*, 2009). Additional charges in the barrel, however, can alter the unitary conductance and rectification properties (Maglia *et al.*, 2008), while the introduction of aromatic residues near the constriction (e.g., M113W and M113Y), or positively charged residues near the *trans* entrance (e.g., T129R and T125R) can produce pores that show a high frequency of gating (M. Rincon-Restrepo, unpublished data). In some cases, the gating events observed with nanopores that have additional positive charge in the barrel might be due to the binding of contaminants to the protein pore (Cheley *et al.*, 2002) as they are more frequent at low salt concentrations when the charges within the pore are less well screened.

## 3.4. Nanopore stability

αHL heptamers in bilayers are stable under extreme conditions of salt concentration, temperature (Kang *et al.*, 2005), pH (Gu and Bayley, 2000; Maglia *et al.*, 2009b), and in the presence of denaturants (Japrung *et al.*, 2010). Pores can insert into bilayers and remain open over a wide range of ionic strengths (from 0.001 to 4 *M* KCl). Throughout this range, the conductance of the pore varies linearly with the ionic concentration of the solution, except at very low salt concentrations where there is a small deviation from linearity (Oukhaled *et al.*, 2008).

Electrical recordings of αHL pores have been carried out from 4 to 93 °C (Kang *et al.*, 2005). Over this range, the conductance of the pore increases roughly linearly, largely reflecting the temperature dependence of the conductivity of the electrolyte. DNA translocation experiments are usually carried out at room temperature, but lower temperatures can be used to reduce the speed of DNA translocation through the pore, by an order of magnitude over a range of 25 °C at +120 mV (Meller *et al.*, 2000), which is most likely an effect of the lowered viscosity. High temperatures might be useful for denaturing DNA during translocation experiments.

Current recordings from αHL pores in symmetric solutions have been performed from pH 4 to 13 (Gu and Bayley, 2000; Maglia *et al.*, 2009b). However, the rate of insertion of preassembled heptamers decreases dramatically at pH values greater than 11 and at pH >11.7 αHL can no longer be transferred into planar lipid bilayers. CD and fluorescence experiments revealed that the cap domain of the protein is unfolded in 0.3% (w/v) SDS at pH 12, suggesting that correct folding of the cap is important for the insertion of αHL heptamers. Once in lipid bilayers, however, αHL pores appear to be more stable than in SDS solution and there is no evidence to suggest that the protein unfolds within the pH range tested. Therefore, to examine αHL at pH >11, the pores must be reconstituted at lower pH and the pH of the solution brought to the desired pH by adding small portions of 1 *M* KOH with stirring. The pH of the *cis* compartment (ground) can be monitored by using a pH electrode. However, measurement of the pH in

the *trans* compartment provokes breaking of the bilayer, unless the *trans* electrode is removed or a conducting bridge is first formed with a Pt wire between the two compartments.

αHL pores are also stable in high concentrations of denaturants (e.g., up to 8 *M* urea), which has been used, for example, to investigate the translocation of unfolded polypeptides (Oukhaled *et al.*, 2007) or to reduce the secondary structure of DNA for translocation (Japrung *et al.*, 2010). Since the insertion of αHL occurs only at concentrations of urea lower than 3 *M*, higher concentrations of denaturants are attained by replacing the buffer after a pore has inserted into a planar bilayer.

## 4. MATERIALS

### 4.1. Buffer components

Typically, DNA translocation experiments are carried out in 1 *M* KCl. Because of possible contaminants, the KCl and other buffer components should be of the highest possible purity. We use KCl from Fluka (catalog no. 05257) which contains less than 0.0005% of trace metals.

### 4.2. Handling of DNA and RNA

In many experiments, synthetic DNAs and RNAs of 50–100 nt are used. The capture of these nucleic acids is inefficient (e.g., $\sim 4$ s$^{-1}$ $\mu M^{-1}$ at $+120$ mV with WT-αHL) (Henrickson *et al.*, 2000; Maglia *et al.*, 2008; Meller, 2003; Nakane *et al.*, 2002). Therefore, DNA or RNA is usually presented at concentrations of $>100$ n*M* and the use of small chambers can help conserve materials (Akeson *et al.*, 1999). Nucleic acids, especially RNA, should be manipulated under nuclease-free conditions. Materials including water, tips, and tubes should be autoclaved prior to use and the experimental area should be cleaned with a product such as RNaseZap (Ambion), to inactivate RNAse. RNaseZap may also be used on the chamber provided it is thoroughly rinsed afterward. Purified RNA can be stored in 50% (v/v) formamide, which is known to protect RNA from degradation (Chomczynski, 1992).

### 4.3. Short single-stranded DNA or RNA

Several companies, such as ATDBio, Sigma Genosys, RNAeasy kit, Integrated DNA Technologies, and Bio-Synthesis, carry out the custom synthesis of nucleic acids of up to 200 nt in length for ssDNA and up to 50 nt for RNA at the micromole level. An advantage of using synthetic oligonucleotides is that they can be chemically modified at their 5′ or 3′

ends and that additional bases, such as $5'$-methylcytosine, can be incorporated at specific sites. Pure oligonucleotides are essential for nanopore investigations and therefore they are usually desalted by the company, purified by HPLC or PAGE as appropriate for the length, and delivered as dried ethanol precipitates. We have also purified desalted short ssDNA (50–100 nt) and ssRNA ($<$ 50 nt) from Sigma Genosys by denaturing, 7 $M$ urea, 8% polyacrylamide gel electrophoresis (PAGE). After electrophoresis, the ssDNA and ssRNA are stained with ethidium bromide (10 $\mu$g ml$^{-1}$) and visualized under a UV transilluminator 2000 (Bio-Rad). The desired band of polyacrylamide is cut out and crushed in water (100 $\mu$l). The gel is separated from the eluted ssDNA by using P6 Micro-Spin chromatography columns (Bio-Rad). Purity is checked by analytical PAGE.

## 4.4. Long single-stranded DNA

The preparation of long ssDNA molecules ($>$ 200 nt) is usually achieved by using asymmetric PCR. dsDNA templates of the desired length (200–8000 bp) and sequence are prepared by cutting a plasmid DNA with the requisite restriction enzymes. The desired dsDNA is purified from the plasmid DNA by PAGE. The template (e.g., $\sim$0.4 $\mu$g of a 1 kb fragment) is then mixed with a 50- to 100-fold excess of a single synthetic primer that is complementary to a specific sequence in the dsDNA template, and 95 asymmetric PCR cycles are carried out (Screaton *et al.*, 1993). Since only one primer is present, ssDNA is generated, which is then separated from the dsDNA template by PAGE. Alternatively, the primer that is used in the asymmetric PCR can be biotinylated, and the ssDNA can be purified by chromatography with immobilized streptavidin (Kai *et al.*, 1997; Pagratis, 1996). Asymmetric PCR produces only one copy of the template in each cycle and the final yield of ssDNA is generally poor (e.g., $\sim$0.2 $\mu$g for the 1 kb template). The DNA is purified by using a 0.8% low-melt agarose gel.

In an alternative method, a dsDNA template (0.4 $\mu$g) is amplified in 35 PCR cycles by using two primers, one of which is protected at the $5'$ end (e.g., with a covalently attached biotin). In this case, amplification is exponential. After 35 cycles, the resulting dsDNA ($\sim$25 $\mu$g from a 50 $\mu$l reaction) is desalted by using a gel filtration column (Micro Bio-Spin P30 Column, Bio-Rad), and concentrated to 300–500 ng $\mu$l$^{-1}$ with a centrifugal vacuum concentrator (SpeedVac, Savant). Then, to obtain ssDNA, the dsDNA is incubated with $\lambda$-exonuclease ($\sim$2 U $\mu$g$^{-1}$ of DNA) for 3 h at 37 °C, which digests the unprotected DNA strand. After further purification by PAGE, up to 2 $\mu$g of ssDNA are obtained from 5 $\mu$g of dsDNA.

## 4.5. Long RNA preparation

Long RNA molecules can be prepared by transcribing a dsDNA template with an RNA polymerase. RNA molecules up to 8000 nt long can be synthesized. Several companies including Promega and Ambion produce *in vitro* transcription (IVT) kits. For example, the T7 RiboMAX$^{TM}$ Express Large Scale RNA Production System kit (Promega) contains materials sufficient for 12 reactions and can synthesize up to 5 $\mu$g of RNA per reaction. When using this kit, the dsDNA template must contain the T7 promoter sequence that is recognized by T7 RNA polymerase. A typical reaction contains linear dsDNA template (8 $\mu$l, $\sim$4 $\mu$g), 2$\times$ buffer (20 $\mu$l, with rNTPs), RNase-free water (10 $\mu$l), and T7 RNA polymerase (2 $\mu$l). The mixture is incubated at 37 $^{\circ}$C for 1 h to produce the desired RNA and then the dsDNA template is digested with RQ1 RNase-free DNase (4 $\mu$l, 1 U $\mu$l$^{-1}$) for 15 min. The digest is brought to 700 $\mu$l by the addition of RNase-free water (up to 100 $\mu$l, RNAeasy kit), buffer RLT (350 $\mu$l, RNAeasy kit) and ethanol (250 $\mu$l, 96–100%). The sample is then loaded onto a RNase Mini spin column (RNAeasy kit) and washed twice with buffer RPE (500 $\mu$l, RNAeasy kit). The desired RNA is eluted with "double sterile" water (50 $\mu$l, RNAeasy kit). The RNA can be purified in a 5% or 8% polyacrylamide gel, or in a 0.8% agarose gel.

## 4.6. Short dsDNA preparation

dsDNA can be prepared by mixing equimolar amounts of two synthetic complementary ssDNAs in exonuclease I buffer (67 m$M$ glycine–KOH, 6.7 m$M$ MgCl$_2$, 10 m$M$ 2–mercaptoethanol, pH 9.4; New England Bio-Labs). To facilitate the annealing process, the temperature is brought to 95 $^{\circ}$C for 1 min and then decreased stepwise to room temperature. At around the calculated annealing temperature (www.basic.northwestern. edu/biotools/oligocalc.html), the temperature is decreased in small steps (e.g., 2 $^{\circ}$C, each held for 1 min). Excess ssDNA is digested by incubation with *E. coli* exonuclease I (20 U, New England BioLabs) for 30 min at 37 $^{\circ}$C. The dsDNA is ethanol precipitated by first adding 0.1 volumes of 3.0 $M$ sodium acetate at pH 5.2, and then 2.5 volumes of cold 95% (v/v) ethanol. The mixture is left at $-20$ $^{\circ}$C for 1 h and then centrifuged at 25,000 $\times$ g for 20 min. The white pellet is washed several times with cold 95% (v/v) ethanol and after drying taken up in 10 m$M$ Tris–HCl 100 $\mu$M EDTA, pH 7.5. Residual low molecular weight contaminants can be removed by passing the DNA solution (maximum 75 $\mu$l) through a Bio-Spin$^{\circledR}$ 30 column (Bio-Rad). The purity of dsDNA is checked by PAGE by using dyes that stain both single- and double-stranded nucleic acids, for example, Stains-All (Sigma-Aldrich).

# 5. DATA ACQUISITION AND ANALYSIS

## 5.1. Data digitization

The ionic current that flows through a nanopore can be measured by using commercial instruments such as the Axopatch 200B patch–clamp amplifier. These instruments transform the continuous analog current signal into an analog voltage signal, which is then fed to a digitizer that converts it into binary numbers with finite resolution (digitization). The digitizer is connected to a computer that converts and displays the digitized current information. We use 132x or 1440A 16-bit digitizers (Molecular Devices), with a dynamic input range of $\pm 10$ V, which divides the signal into $2^{16}$ (65,536) values (bins), providing a resolution of 0.305 mV/bin (20 V/$2^{16}$). If no output gain is applied, this corresponds to a dynamic range of $\pm 10$ nA and a resolution of 0.305 pA/bin. However, the output gain can be changed (by up to 500-fold) to increase the resolution (decreased bin width), at the expense of dynamic range. Typically, when measuring the translocation of DNA molecules through a single αHL nanopore the output gain is set to at least 10×, which corresponds to a dynamic range of 1 nA and a resolution of 0.0305 pA/bin.

## 5.2. Filtering and sampling

The signal collected by the amplifier must be filtered to remove high–frequency electrical noise. The most common filtering is low-pass filtering, which limits the bandwidth of the data by eliminating signals above the corner frequency (or cutoff frequency) of the filter. Bessel filters, rather than Butterworth filters, are usually applied for time–domain analyses, as Bessel filters are better at preserving the shape of the single-channel response (The Axon Guide) (Silberberg and Magleby, 1993). It is important to select the correct corner frequency and in order to keep errors in estimates of current levels to $< 3\%$, the applied filter cutoff should be greater than five times the inverse of the mean event time (Silberberg and Magleby, 1993). For example, the most probable translocation time for a 92–nt DNA strand through the WT-αHL, at $+ 120$ mV in 1 $M$ KCl, 25 m$M$ Tris–HCl at pH 8, is 0.141 ms (Maglia *et al.*, 2008). Therefore, the cutoff frequency should be $\sim 35$ kHz or higher (Fig. 22.8A). Over-filtering of the signal can lead to inaccurate estimates of $I_B$ and $t_t$ (Fig. 22.8B). As well as the appropriate filtering rate, it is important to select the correct sampling rate. The Nyquist Sampling Theorem states that the sampling rate should be twice the cutoff frequency of the applied filter (The Axon Guide). In practice, however, it is preferable to oversample (i.e., sample at a rate that exceeds the Nyquist minimum) (Sakmann and Neher, 1995). A sampling rate of 10 times that of
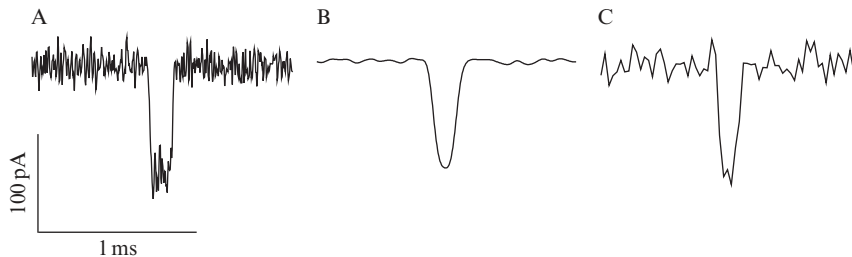
**Figure 22.8** The effects of the filter cutoff frequency and sampling rate on the recording of DNA translocation events. The $t_t$ for each event is $\sim 0.14$ ms suggesting a filter cutoff of $\sim 35$ kHz (see the text). (A) Signal filtered at 40 kHz with a low-pass 8-pole Bessel filter, and sampled at 250 kHz. The filtering and sampling allow faithful reproduction of the translocation event. (B) The event shown in panel A is filtered at 5 kHz. The sampling rate remains 250 kHz. $I_B$ and $t_t$ can no longer be determined accurately. (C) In this case, although the correct level of filtering has been applied (40 kHz), the signal is sampled at the suboptimal rate of 40 kHz.

the cutoff frequency of the filter is desirable, but five times the cutoff frequency is usually sufficient.

## 5.3. Acquisition protocols

The software we use to collect and display the current signals is Clampex from Molecular Devices; however, other software such as QuB (www.qub.buffalo.edu) and WinEDR (http://spider.science.strath.ac.uk/sipbs/page.php?show=software_winEDR) can be used. Clampex can also control the 132x or 1440A digitizer to apply a potential through the amplifier (see below). Although Clampex has five data acquisition modes, the most commonly used during DNA translocation experiments, are the ''Gap Free,'' ''Variable-Length Events,'' and ''Episodic Stimulation'' modes.

In the Gap Free protocol, data are passively and continuously digitized, displayed, and saved. There are no interruptions to the data record, which make it a useful protocol to use when preparing data for publication. However, it should not be used routinely when acquiring with a high sampling rate, or for a long period of time, as the file sizes can become very large (e.g., acquiring at 250 kHz for 1 h will produce a 1.7 GB file).

The Variable-Length Events protocol is ideal for collecting data from a fully characterized system where the frequency of events is very low, and there are long periods of inactivity. Data are visualized as in the gap free protocol, but are acquired only for as long as an input signal has passed a threshold level (which is set manually), so only the ''events'' and small sections on either side of them are recorded. The file sizes are therefore more manageable, although the data record is interrupted.
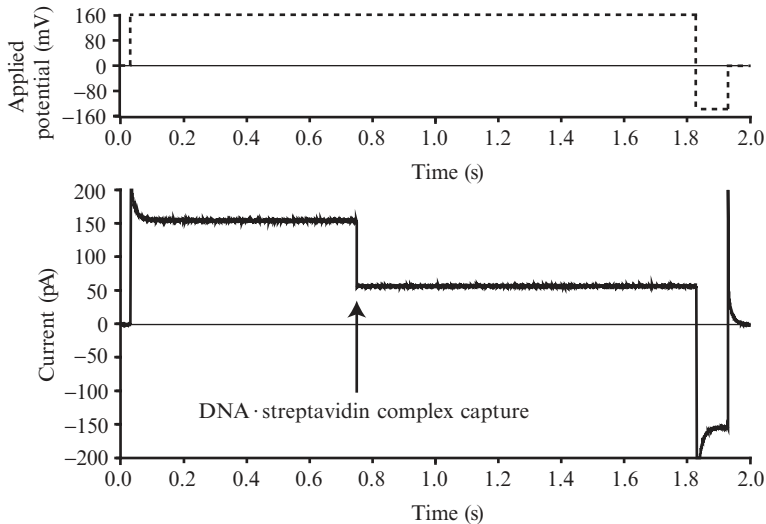
**Figure 22.9** Episodic stimulation mode allows both an output voltage (dashed line) to be applied, while simultaneously recording the resulting changes in ionic current. In this example, a positive potential bias of $+160$ mV is applied to the system, resulting in an open pore current level of $\sim 160$ pA. Under the applied potential, a DNA molecule is driven into the pore and becomes immobilized (through a terminal biotin·streptavidin complex), and the current level is reduced. The potential bias is reversed ($-140$ mV) and the DNA molecule is ejected. The bias is then removed. The protocol can be repeated numerous times.

The Episodic Stimulation protocol can be used to output a voltage signal from the digitizer, which can be applied to the bilayer system, while simultaneously acquiring the resulting current signal. This mode is used to apply voltage steps (e.g., when producing *I–V* curves) or voltage ramps (Dudko *et al.*, 2007). It can also be used when it is laborious to apply different voltages manually with the patch–clamp amplifier, for example, when studying the repeated immobilization of DNA molecules inside the αHL pore. In this case, a voltage bias can be applied, for a fixed amount of time, to drive a DNA·streptavidin complex into the pore. The bias is then reversed to eject the molecule from the pore (Fig. 22.9) (Purnell *et al.*, 2008; Stoddart *et al.*, 2009, 2010). The changes in the current level that occur as a result of the voltage protocol are simultaneously acquired. The protocol can be repeated hundreds of times per run and therefore many DNA blockades can be recorded. The output waveform can be set manually to apply different voltage steps, for different times, and it does not have to be the same for each sweep during a run.

## 5.4. Analysis of single DNA/RNA molecules

The current traces recorded by the digitizer can be analyzed by using the "single-channel search" option in the Clampfit software package (Molecular Devices). In doing so, the user must assign the value of the open pore current
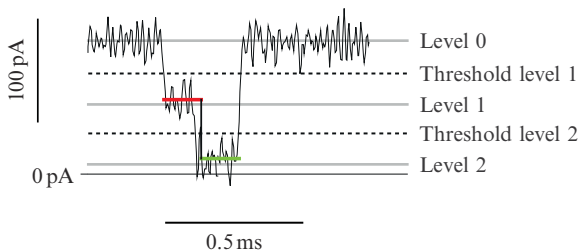
**Figure 22.10** Typical DNA translocation event analyzed by the Clampfit software. Levels 0, 1, and 2 are set manually and the software automatically assigns data points to level 1 (red line) or level 2 (green line).

(level 0) and a second level (level 1) that corresponds to the blocked pore level. If a DNA molecule provokes several types of current blockade, of differing amplitude, additional levels can be assigned (levels 2, 3, ..., etc.). Every time the ionic current crosses a threshold (the half distance between two levels), the software recognizes it as an "event"( Fig. 22.10) and records its characteristics such as the mean amplitude, the dwell time, and the interevent interval in a results window. Generally, for short DNA molecules, the average current amplitudes, dwell times, and interevent intervals of numerous events are plotted as histograms. Gaussian fits to the events histogram of the amplitudes and dwell times are used to determine $I_B$ and $t_P$, respectively; while $\bar{t}_{ON}$ is determined from an exponential fit to the histogram of the interevent intervals. The dwell times ($t_D$) are described by a Gaussian distribution with an exponential tail; the peak of the Gaussian ($t_P$) is generally used to describe the most likely dwell time, which often represents the translocation time, $t_t$ (Meller *et al.*, 2000). In the case of DNA strands immobilized within a nanopore, $I_B$ values are the only meaningful features of the events (Ashkenasy *et al.*, 2005; Purnell and Schmidt, 2009; Stoddart *et al.*, 2009).

## REFERENCES

Akeson, M., Branton, D., Kasianowicz, J. J., Brandin, E., and Deamer, D. W. (1999). Microsecond time-scale discrimination among polycytidylic acid, polyadenylic acid and polyuridylic acid as homopolymers or as segments within single RNA molecules. *Biophys. J.* **77,** 3227–3233.

Ashkenasy, N., Sánchez-Quesada, J., Bayley, H., and Ghadiri, M. R. (2005). Recognizing a single base in an individual DNA strand: A step toward nanopore DNA sequencing. *Angew. Chem. Int. Ed. Engl.* **44,** 1401–1404.

Astier, Y., Kainov, D. E., Bayley, H., Tuma, R., and Howorka, S. (2007). Stochastic detection of motor protein–RNA complexes by single-channel current recording. *ChemPhysChem* **8,** 2189–2194.

Bayley, H. (2006). Sequencing single molecules of DNA. *Curr. Opin. Chem. Biol.* **10,** 628–637.

Bayley, H., and Cremer, P. S. (2001). Stochastic sensors inspired by biology. *Nature* **413,** 226–230.

Bayley, H., Cronin, B., Heron, A., Holden, M. A., Hwang, W., Syeda, R., Thompson, J., and Wallace, M. (2008a). Droplet interface bilayers. *Mol. BioSyst.* **4,** 1191–1208.

Bayley, H., Luchian, T., Shin, S.-H., and Steffensen, M. B. (2008b). Single-molecule covalent chemistry in a protein nanoreactor. *In* "Single Molecules and Nanotechnology," (R. Rigler and H. Vogel, eds.), pp. 251–277. Springer, Heidelberg.

Bezrukov, S. M., and Kasianowicz, J. J. (1993). Current noise reveals protonation kinetics and number of ionizable sites in an open protein ion channel. *Phys. Rev. Lett.* **70,** 2352–2355.

Bhakdi, S., Füssle, R., and Tranum-Jensen, J. (1981). Staphylococcal α-toxin: Oligomerization of hydrophilic monomers to form amphiphilic hexamers induced through contact with deoxycholate micelles. *Proc. Natl. Acad. Sci. USA* **78,** 5475–5479.

Bonthuis, D. J., Zhang, J., Hornblower, B., Mathe, J., Shklovskii, B. I., and Meller, A. (2006). Self-energy-limited ion transport in subnanometer channels. *Phys. Rev. Lett.* **97,** 128104.

Branton, D., Deamer, D. W., Marziali, A., Bayley, H., Benner, S. A., Butler, T., Di Ventra, M., Garaj, S., Hibbs, A., Huang, X., Jovanovich, S. B., Krstic, P. S., *et al.* (2008). The potential and challenges of nanopore sequencing. *Nat. Biotechnol.* **26,** 1146–1153.

Butler, T. Z., Gundlach, J. H., and Troll, M. (2007). Ionic current blockades from DNA and RNA molecules in the alpha-hemolysin nanopore. *Biophys. J.* **93,** 3229–3240.

Butler, T. Z., Pavlenok, M., Derrington, I. M., Niederweis, M., and Gundlach, J. H. (2008). Single-molecule DNA detection with an engineered MspA protein nanopore. *Proc. Natl. Acad. Sci. USA* **105,** 20647–20652.

Cheley, S., Malghani, M. S., Song, L., Hobaugh, M., Gouaux, J. E., Yang, J., and Bayley, H. (1997). Spontaneous oligomerization of a staphylococcal α–hemolysin conformationally constrained by removal of residues that form the transmembrane β barrel. *Protein Eng.* **10,** 1433–1443.

Cheley, S., Braha, O., Lu, X., Conlan, S., and Bayley, H. (1999). A functional protein pore with a "retro" transmembrane domain. *Protein Sci.* **8,** 1257–1267.

Cheley, S., Gu, L.-Q., and Bayley, H. (2002). Stochastic sensing of nanomolar inositol 1,4,5-trisphosphate with an engineered pore. *Chem. Biol.* **9,** 829–838.

Chomczynski, P. (1992). Solubilization in formamide protects RNA from degradation. *Nucleic Acids Res.* **20,** 3791–3792.

Clarke, J., Wu, H., Jayasinghe, L., Patel, A., Reid, S., and Bayley, H. (2009). Continuous base identification for single-molecule nanopore DNA sequencing. *Nat. Nanotechnol.* **4,** 265–270.

Cockroft, S. L., Chu, J., Amorin, M., and Ghadiri, M. R. (2008). A single-molecule nanopore device detects DNA polymerase activity with single-nucleotide resolution. *J. Am. Chem. Soc.* **130,** 818–820.

Deamer, D. W., and Branton, D. (2002). Characterization of nucleic acids by nanopore analysis. *Acc. Chem. Res.* **35,** 817–825.

Dekker, C. (2007). Solid-state nanopores. *Nat. Nanotechnol.* **2,** 209–215.

Dudko, O. K., Mathe, J., Szabo, A., Meller, A., and Hummer, G. (2007). Extracting kinetics from single-molecule force spectroscopy: Nanopore unzipping of DNA hairpins. *Biophys. J.* **92,** 4188–4195.

Gillis, K. D. (1995) *In* "Techniques for membrane capacitance measurements," (B. Sakmann, and E. Neher, ed), pp. 155, Vol. 2. Plenum, New York.

Gu, L. Q., and Bayley, H. (2000). Interaction of the non-covalent molecular adapter, b-cyclodextrin, with the staphylococcal α–hemolysin pore. *Biophys. J.* **79,** 1967–1975.

Gu, L. Q., Cheley, S., and Bayley, H. (2001). Prolonged residence time of a noncovalent molecular adapter, *β*-cyclodextrin, within the lumen of mutant α–hemolysin pores. *J. Gen. Physiol.* **118,** 481–494.

Hanke, W., and Schlue, W.-R. (1993). Planar Lipid Bilayers. Academic Press, London.

Henrickson, S. E., Misakian, M., Robertson, B., and Kasianowicz, J. J. (2000). Driven DNA transport into an asymmetric nanometer-scale pore. *Phys. Rev. Lett.* **85,** 3057–3060.

Holden, M. A., and Bayley, H. (2005). Direct introduction of single protein channels and pores into lipid bilayers. *J. Am. Chem. Soc.* **127,** 6502–6503.

Holden, M. A., Jayasinghe, L., Daltrop, O., Mason, A., and Bayley, H. (2006). Direct transfer of membrane proteins from bacteria to planar bilayers for rapid screening by single-channel recording. *Nat. Chem. Biol.* **2,** 314–318.

Hornblower, B., Coombs, A., Whitaker, R. D., Kolomeisky, A., Picone, S. J., Meller, A., and Akeson, M. (2007). Single-molecule analysis of DNA–protein complexes using nanopores. *Nat. Methods* **4,** 315–317.

Howorka, S., Cheley, S., and Bayley, H. (2001). Sequence-specific detection of individual DNA strands using engineered nanopores. *Nat. Biotechnol.* **19,** 636–639.

Hung, W. C., Chen, F. Y., and Huang, H. W. (2000). Order–disorder transition in bilayers of diphytanoyl phosphatidylcholine. *Biochim. Biophys. Acta* **1467,** 198–206.

Japrung, D., Henricus, M., Li, Q., Maglia, G., and Bayley, H. (2010). Urea facilitates the translocation of single-stranded DNA and RNA through the α-hemolysin nanopore. *Biophys. J.* **98,** 1856–1863.

Kado, R. T. (1993). Membrane area and electrical capacitance. *Methods Enzymol.* **221,** 273–299.

Kai, E., Sawata, S., Ikebukuro, K., Iida, T., Honda, T., and Karube, I. (1997). Novel DNA detection system of flow injection analysis (2). The distinctive properties of a novel system employing PNA (peptide nucleic acid) as a probe for specific DNA detection. *Nucleic Acids Symp. Ser.* 321–322.

Kang, X., Gu, L.-Q., Cheley, S., and Bayley, H. (2005). Single protein pores containing molecular adapters at high temperatures. *Angew. Chem. Int. Ed. Engl.* **44,** 1495–1499.

Kasianowicz, J. J., Brandin, E., Branton, D., and Deamer, D. W. (1996). Characterization of individual polynucleotide molecules using a membrane channel. *Proc. Natl. Acad. Sci. USA* **93,** 13770–13773.

Kawano, R., Schibel, A. E., Cauley, C., and White, H. S. (2009). Controlling the translocation of single-stranded DNA through alpha-hemolysin ion channels using viscosity. *Langmuir* **25,** 1233–1237.

Keyser, U. F., Koeleman, B. N., van Dorp, S., Krapf, D., Smeets, R. M. M., Lemay, S. G., Dekker, N. H., and Dekker, C. (2006). Direct force measurements on DNA in a solid-state nanopore. *Nat. Phys.* **2,** 473–477.

Korchev, Y. E., Bashford, C. L., Alder, G. M., Apel, P. Y., Edmonds, D. T., Lev, A. A., Nandi, K., Zima, A. V., and Pasternak, C. A. (1997). A novel explanation for fluctuations of ion current through narrow pores. *FASEB J.* **11,** 600–608.

Krasne, S., Eisenman, G., and Szabo, G. (1971). Freezing and melting of lipid bilayers and the mode of action of nonactin, valinomycin, and gramicidin. *Science* **174,** 412–415.

Lindsey, H., Petersen, N. O., and Chan, S. I. (1979). Physicochemical characterization of 1,2-diphytanoyl-sn-glycero-3-phosphocholine in model membrane systems. *Biochim. Biophys. Acta* **555,** 147–167.

Maglia, G., Rincon Restrepo, M., Mikhailova, E., and Bayley, H. (2008). Enhanced translocation of single DNA molecules through α-hemolysin nanopores by manipulation of internal charge. *Proc. Natl. Acad. Sci. USA* **105,** 19720–19725.

Maglia, G., Heron, A. J., Hwang, W. L., Holden, M. A., Mikhailova, E., Li, Q., Cheley, S., and Bayley, H. (2009a). Droplet networks with incorporated protein diodes show collective properties. *Nat. Nanotechnol.* **4,** 437–440.

Maglia, M., Henricus, M., Wyss, R., Li, Q., Cheley, S., and Bayley, H. (2009b). DNA strands from denatured duplexes are translocated through engineered protein nanopores at alkaline pH. *Nano Lett.* **9,** 3831–3836.

Martin, H., Kinns, H., Mitchell, N., Astier, Y., Madathil, R., and Howorka, S. (2007). Nanoscale protein pores modified with PAMAM dendrimers. *J. Am. Chem. Soc.* **129,** 9640–9649.

Mayer, M., Kriebel, J. K., Tosteson, M. T., and Whitesides, G. M. (2003). Microfabricated teflon membranes for low-noise recordings of ion channels in planar lipid bilayers. *Biophys. J.* **85,** 2684–2695.

Meller, A. (2003). Dynamics of polynucleotide transport through nanometre-scale pores. *J. Phys.: Condens. Matter* **15,** R581–R607.

Meller, A., and Branton, D. (2002). Single molecule measurements of DNA transport through a nanopore. *Electrophoresis* **23,** 2583–2591.

Meller, A., Nivon, L., Brandin, E., Golovchenko, J., and Branton, D. (2000). Rapid nanopore discrimination between single polynucleotide molecules. *Proc. Natl. Acad. Sci. USA* **97,** 1079–1084.

Meller, A., Nivon, L., and Branton, D. (2001). Voltage-driven DNA translocations through a nanopore. *Phys. Rev. Lett.* **86,** 3435–3438.

Miles, G., Bayley, H., and Cheley, S. (2002). Properties of *Bacillus cereus* hemolysin II: A heptameric transmembrane pore. *Protein Sci.* **11,** 1813–1824.

Miller, C. (ed.), (1986). Ion Channel Reconstitution. Plenum, New York.

Mitchell, N., and Howorka, S. (2008). Chemical tags facilitate the sensing of individual DNA strands with nanopores. *Angew. Chem. Int. Ed. Engl.* **47,** 5565–5568.

Montal, M., and Mueller, P. (1972). Formation of bimolecular membranes from lipid monolayers and study of their electrical properties. *Proc. Natl. Acad. Sci. USA* **69,** 3561–3566.

Morera, F. J., Vargas, G., Gonzalez, C., Rosenmann, E., and Latorre, R. (2007). Ion-channel reconstitution. *Methods Mol. Biol.* **400,** 571–585.

Nakane, J., Akeson, M., and Marziali, A. (2002). Evaluation of nanopores as candidates for electronic analyte detection. *Electrophoresis* **23,** 2592–2601.

Nakane, J., Wiggin, M., and Marziali, A. (2004). A nanosensor for transmembrane capture and identification of single nucleic acid molecules. *Biophys. J.* **87,** 615–621.

Niles, W. D., Levis, R. A., and Cohen, F. S. (1988). Planar bilayer membranes made from phospholipid monolayers form by a thinning process. *Biophys. J.* **53,** 327–335.

Oukhaled, G., Mathé, J., Biance, A.-L., Bacri, L., Betton, J.-M., Lairez, D., Pelta, J., and Auvray, L. (2007). Unfolding of proteins and long transient conformations detected by single nanopore recording. *Phys. Rev. Lett.* **98,** 158101.

Oukhaled, G., Bacri, L., Mathé, J., Pelta, J., and Auvray, L. (2008). Effect of screening on the transport of polyelectrolytes through nanopores. *Europhys. Lett.* **82,** 48003(1–5).

Pagratis, N. C. (1996). Rapid preparation of single stranded DNA from PCR products by streptavidin induced electrophoretic mobility shift. *Nucleic Acids Res.* **24,** 3645–3646.

Peng, H., and Ling, X. S. (2009). Reverse DNA translocation through a solid-state nanopore by magnetic tweezers. *Nanotechnology* **20,** 185101.

Peterman, M. C., Ziebarth, J. M., Braha, O., Bayley, H., Fishman, H. A., and Bloom, D. A. (2002). Ion channels and lipid bilayer membranes under high potentials using micro-fabricated apertures. *Biomed. Microdevices* **4,** 231–236.

Phillips, R., Ursell, T., Wiggins, P., and Sens, P. (2009). Emerging roles for lipids in shaping membrane–protein function. *Nature* **459,** 379–385.

Purnell, R. F., Mehta, K. K., and Schmidt, J. J. (2008). Nucleotide identification and orientation discrimination of DNA homopolymers immobilized in a protein nanopore. *Nano Lett.* **9,** 3029–3034.

Purnell, R. F., and Schmidt, J. J. (2009). Discrimination of single base substitutions in a DNA strand immobilized in a biological nanopore. *ACS Nano* **3,** 2533–2538.

Purves, R. D. (1981). Microelectrode Methods for Intracellular Recording and Ionophoresis. Academic Press.

Rhee, M., and Burns, M. A. (2007). Nanopore sequencing technology: Nanopore preparations. *Trends Biotechnol.* **25,** 174–181.

Rincon-Restrepo, M., Mikhailova, E., Bayley, H., and Maglia, G. Controlled translocation of single DNA molecules through engineered protein nanopores. In preparation.

Sakmann, B., and Neher, B. (1995). Single-Channel Recording. Plenum, New York.

Screaton, G. R., Bangham, C. R., and Bell, J. I. (1993). Direct sequencing of single primer PCR products: A rapid method to achieve short chromosomal walks. *Nucleic Acids Res.* **21,** 2263–2264.

Sexton, L. T., Horne, L. P., and Martin, C. R. (2007). Developing synthetic conical nanopores for biosensing applications. *Mol. BioSyst.* **3,** 667–685.

Silberberg, S. D., and Magleby, K. L. (1993). Preventing errors when estimating single channel properties from the analysis of current fluctuations. *Biophys. J.* **65,** 1570–1584.

Song, L., Hobaugh, M. R., Shustak, C., Cheley, S., Bayley, H., and Gouaux, J. E. (1996). Structure of staphylococcal α-hemolysin, a heptameric transmembrane pore. *Science* **274,** 1859–1865.

Stoddart, D., Heron, A., Mikhailova, E., Maglia, G., and Bayley, H. (2009). Single nucleotide discrimination in immobilized DNA oligonucleotides with a biological nanopore. *Proc. Natl. Acad. Sci. USA* **106,** 7702–7707.

Stoddart, D., Maglia, G., Mikhailova, E., Heron, A., and Bayley, H. (2010). Multiple base-recognition sites in a biological nanopore—Two heads are better than one. *Angew. Chem. Int. Ed.* **49,** 556–559.

Tobkes, N., Wallace, B. A., and Bayley, H. (1985). Secondary structure and assembly mechanism of an oligomeric channel protein. *Biochemistry* **24,** 1915–1920.

Vercoutere, W., Winters-Hilt, S., Olsen, H., Deamer, D., Haussler, D., and Akeson, M. (2001). Rapid discrimination among individual DNA hairpin molecules at single-nucleotide resolution using an ion channel. *Nat. Biotechnol.* **19,** 248–252.

White, S. (1975). Phase transitions in planar bilayer membranes. *Biophys. J.* **15,** 95–117.

White, S. H. (1986). *In* "The Physical Nature of Planar Lipid Membranes Ion Channel Reconstitution," (C. Miller, ed.), pp. 3–35. Plenum, New York.

White, S. H., Petersen, D. C., Simon, S., and Yafuso, M. (1976). Formation of planar bilayer membranes from lipid monolayers. A critique. *Biophys. J.* **16,** 481–489.

Wonderlin, W. F., Finkel, A., and French, R. J. (1990). Optimizing planar lipid bilayer single-channel recordings for high resolution with rapid voltage steps. *Biophys. J.* **58,** 289–294.